European Radiology (2019) 29:5889–5900
https://doi.org/10.1007/s00330-019-06192-x

MAGNETIC RESONANCE

Is liver lesion characterisation by simplified IVIM DWI also feasible at 3.0 T?

Petra Mürtz[1,2] · C. C. Pieper[1] · M. Reick[1] · A. M. Sprinkart[1] · H. H. Schild[1] · W. A. Willinek[1] · G. M. Kukuk[1]

Received: 8 November 2018 / Revised: 25 February 2019 / Accepted: 20 March 2019 / Published online: 8 April 2019

Abstract

Objective To evaluate simplified intravoxel incoherent motion (IVIM) diffusion-weighted imaging (DWI) for liver lesion characterisation at 3.0 T and to compare it with 1.5 T.

Methods 3.0-T DWI data from a respiratory-gated MRI sequence with $b = 0$, 50, 250, and 800 s/mm^2 were analysed in 116 lesions (78 patients) and 27 healthy livers. Apparent diffusion coefficient ADC = ADC(0,800) and IVIM-based parameters $D_1' =$ ADC(50,800), $D_2' =$ ADC(250,800), $f_1' = f$(0,50,800), $f_2' = f$(0,250,800), $D^{*\prime} = D^*$(0,50,250,800), $\mathrm{ADC_{low}} =$ ADC(0,50), and $\mathrm{ADC_{diff}} = \mathrm{ADC_{low}}$-$D_2'$ were calculated voxel-wise and analysed on per-patient basis. Results were compared with those of 173 lesions (110 patients) and 40 healthy livers at 1.5 T.

Results Focal nodular hyperplasias were best discriminated from all other lesions by f_1' and haemangiomas by D_1' with an area under the curve (AUC) of 0.993 and 1.000, respectively. For discrimination between malignant and benign lesions, ADC was best suited (AUC of 0.968). The combination of D_1' and f_1' correctly identified more lesions as malignant or benign than the ADC (99.1% vs 88.8%). Discriminatory power for differentiating malignant from benign lesions tended to be higher at 3.0 T than at 1.5 T.

Conclusion Simplified IVIM is suitable for lesion characterisation at 3.0 T with a trend of superior diagnostic accuracy for discriminating malignant from benign lesions compared with 1.5 T.

Key Points

- *Simplified IVIM is also suitable for liver lesion characterisation at 3.0 T.*
- *Excellent accuracy was reached for discriminating malignant from benign lesions.*
- *The acquisition of only three b-values (0, 50, 800 s/mm^2) is required.*

Keywords Diffusion magnetic resonance imaging · Carcinoma, hepatocellular · Liver neoplasms · Haemangioma · Focal nodular hyperplasia

Abbreviations

ADC	Apparent diffusion coefficient
AUC	Area under the curve
CCC	Cholangiocellular carcinoma
DWI	Diffusion-weighted imaging
FNH	Focal nodular hyperplasia
HCC	Hepatocellular carcinoma
IVIM	Intravoxel incoherent motion
REF	Reference tissue
ROI	Region of interest

P. Mürtz and C.C. Pieper contributed equally to this work.

✉ Petra Mürtz
petra.muertz@ukb.uni-bonn.de

[1] Department of Radiology, University of Bonn, Bonn, Germany

[2] Radiologische Klinik der Universität Bonn, Sigmund-Freud-Straße 25, 53105 Bonn, Germany

Introduction

In diffusion-weighted imaging (DWI), the intravoxel incoherent motion (IVIM) concept of Le Bihan [1] proposes a separate analysis of diffusion and perfusion effects by using a bi-exponential model. The acquisition of at least four *b*-values allows the determination of the true diffusion coefficient *D*,

the perfusion fraction *f*, and the pseudodiffusion coefficient *D** [2]. *D* represents the mobility of water molecules in tissue [3–6], *f* reflects the relative contribution of microvascular blood flow to the DWI signal, and *D** depends on blood velocity and length of microvessel segments [1, 2, 7].

The role of IVIM imaging for lesion characterisation is still subject of investigation and remains controversially discussed [8–19]. A known problem is limited stability of IVIM analysis in case of low *D** and/or *f* values as found in some malignant lesions and haemangiomas [8, 9, 16, 20, 21]. If *D** is low (i.e. in the order of *D*), the signal decay is hardly bi-exponential. In cases with low *f*, the total IVIM effect can be very small. In both cases, the simultaneous determination of *D*, *f*, and *D** by using unconstrained non-linear least squares fitting procedures leads to numerical instabilities, poor reproducibility of *D** and *f*, and unreliable results [20, 21]. Improved stability can be achieved for IVIM approaches using a two-step constrained analysis methods like segmented fitting [9, 14, 16] and simplified IVIM [8, 15, 17, 22–25]. In simplified IVIM, explicit approximation formulas in combination with low number of acquired *b*-values are used. Thus, simplified IVIM is generally suitable for clinical routine applications. Recently, basic investigations were published for liver lesion characterisation at 1.5 T using a simplified IVIM approach with four *b*-values [8]. Data on simplified IVIM approaches at 3.0 T and comparisons on IVIM at 1.5 and 3.0 T are still missing.

Thus, the aim of this study was to perform basic investigations of simplified IVIM based on four *b*-values for liver lesion characterisation at 3.0 T and to compare results with 1.5 T in terms of optimal *b*-values, most suited IVIM parameters, threshold values, and accuracy.

Materials and methods

Subjects

DWI data of consecutive clinical routine liver examinations from August 2012 to July 2016 acquired with four *b*-values at 3.0 T were reviewed. The study was approved by the local institutional review board of the University Hospital Bonn, which waived the need for informed patient consent because it was a retrospective analysis study of clinical routine examinations. One hundred forty-eight patients fulfilled the inclusion criterion of at least one focal hepatic lesion ≥ 1 cm detected in the examination using all available sequences. Seventy patients were excluded as outlined in Fig. 1 and data of 78 patients were finally analysed (Table 1). Diagnosis of liver lesions was undertaken within clinical routine. Cholangiocellular carcinomas (CCCs) were histologically proven. Hepatocellular carcinomas (HCCs) were either histologically proven or diagnosed according to the American Association for the Study for Liver Disease MRI criteria [26]. Diagnosis of metastasis was based on typical imaging features in combination with histologically proven primary cancer. Diagnosis of focal nodular hyperplasia (FNH) or haemangioma was established on the basis of typical radiological findings on contrast-enhanced MRI and was confirmed by at least one follow-up examination. In addition, healthy liver parenchyma, defined as normal appearing liver in MRI in combination with clinically absent liver disease, was investigated in 27 patients (Table 1), which served as reference (REFs). Hereby, 5 patients of the benign lesion groups were included who had no other liver disease based on clinical and radiological data. In addition, 22 randomly selected patients with non-specific abdominal symptoms or non-conclusive sonographic examinations and normal hepatic MRI examinations without liver disease and without malignant disease were included.

In addition to the 3.0-T data, the data of a different patient group (110 patients with liver lesions and 40 patients with healthy liver based on clinical and radiological criteria), which were examined with simplified IVIM at 1.5 T in a previous study [8], were included (see Fig. 1 and Table 1). In the previous study, basic investigations concerning simplified IVIM at 1.5 T had been performed, whereas in the present study, the data were used to analyse the diagnostic yield of simplified IVIM at 3.0 T in comparison with 1.5 T.

Magnetic resonance imaging

All examinations were performed on a clinical 3.0-T MRI system (Ingenia, 3.0 T, Philips Healthcare, gradient system: 80 mT/m maximum amplitude, 200 T/m/s maximum slew rate; equipped with dual-source RF transmission technology) using commercially available phased array surface coils for signal detection. As in the previous study [8], the DWI sequence (Table 2) was a respiratory-triggered single-shot spin-echo echo-planar imaging variant with four *b*-values (0, 50, 250, and 800 s/mm^2). It was part of the standardised imaging protocol and always acquired before contrast agent injection. Isotropic (directionally independent) diffusion-weighted images were reconstructed from the images with diffusion-sensitised gradients in three orthogonal directions on the MRI system.

Postprocessing of the 3.0-T data

As in reference [8], two different approximations of *D* and *f* were calculated from the acquired *b*-values, one from $b_0 = 0$, $b_1 = 50$, $b_3 = 800$ and one from $b_0 = 0$, $b_2 = 250$, $b_3 = 800$ s/mm^2:

$$D_1' = ADC(50, 800) = \frac{\ln(S(b_1)) - \ln(S(b_3))}{b_3 - b_1} \quad (1)$$

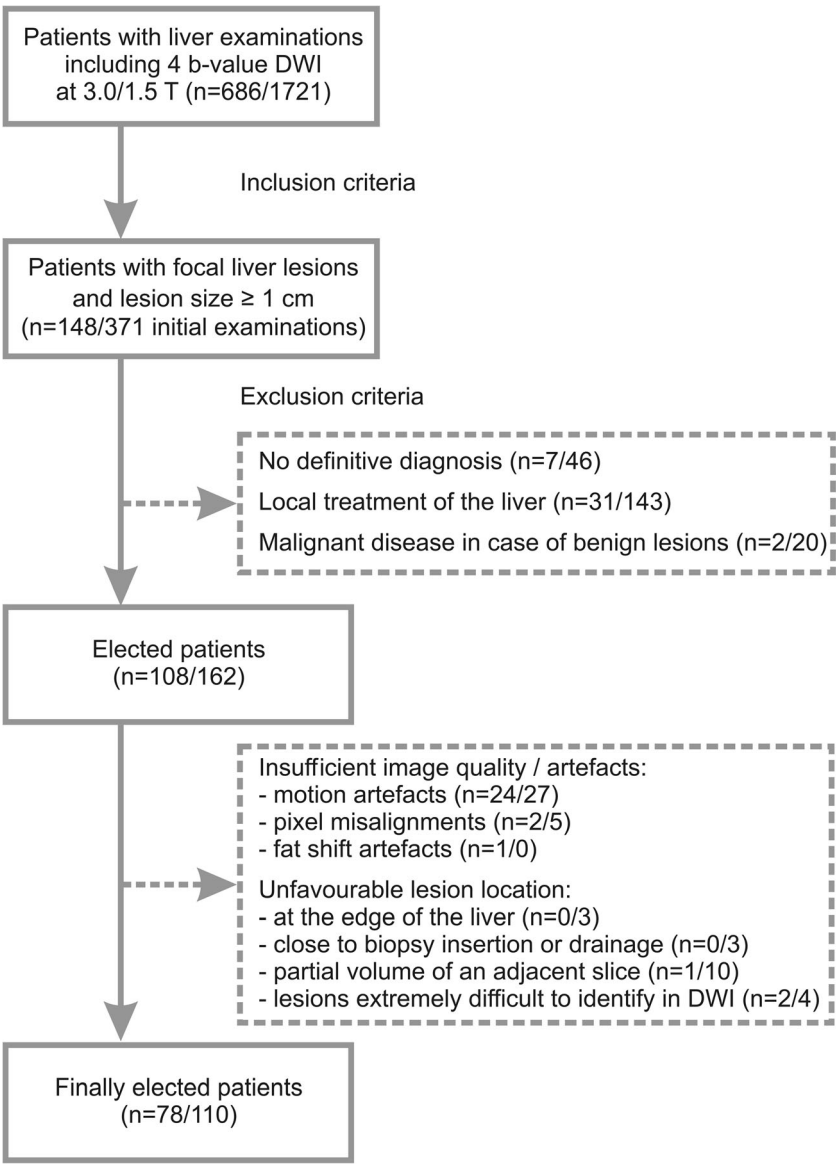

Fig. 1 Flow chart of inclusion and exclusion criteria of the study sample

$$D_2' = ADC(250,800) = \frac{\ln(S(b_2)) - \ln(S(b_3))}{b_3 - b_2} \quad (2)$$

$$f_1' = f(0,50,800) = 1 - \frac{S(b_1)}{S(0)} \cdot \exp^{D_1' \cdot b_1} \quad (3)$$

$$f_2' = f(0,250,800) = 1 - \frac{S(b_2)}{S(0)} \cdot \exp^{D_2' \cdot b_2} \quad (4)$$

From the four *b*-values, *D** was approximated by using D_2' and f_2' and the reading for b_1:

$$D^{*'} = D^*(0,50,250,800) = -\frac{1}{b_1} \cdot \ln\left[\frac{1}{f_2'} \cdot \left(\frac{S(b_1)}{S(0)} - \left(1 - f_2'\right) \cdot \exp^{-D_2' \cdot b_1}\right)\right] \quad (5)$$

Moreover, the perfusion-sensitive parameters ADC_{low} and ADC_{diff} and the conventional ADC were calculated:

$$ADC_{low} = ADC(0,50) = \frac{\ln(S(b_0)) - \ln(S(b_1))}{b_1 - b_0} \quad (6)$$

$$ADC_{diff} = ADC_{low} - D_2' \quad (7)$$

$$ADC = ADC(0,800) = \frac{\ln(S(b_0)) - \ln(S(b_3))}{b_3 - b_0} \quad (8)$$

Parameter maps were calculated offline in MATLAB (MathWorks).

Analysis of IVIM parameters at 3.0 T

Image analyses were performed in consensus by a board-certified radiologist with more than 14 years of experience in abdominal imaging and a physicist with more than 19 years of experience in DWI. For each lesion included, one region of interest (ROI) was analysed in a single slice

Table 1 Group composition and demographic data of included subjects at 3.0 and 1.5 T

Patients with	3.0 T				1.5 T			
	Total number	Number of males	Age (MV ± SD) (years)	Age range (years)	Total number	Number of males	Age (MV ± SD) (years)	Age range (years)
HCCs	30	25	69 ± 9	50–87	32	20	71 ± 9	55–87
CCCs	5	3	72 ± 3	68–76	8	4	69 ± 10	57–85
CRCs	13	8	63 ± 8	52–81	22	17	60 ± 10	47–87
BCs	10	0	57 ± 9	45–72	12	0	60 ± 6	48–70
Haemangiomas	12	5	47 ± 12	32–72	23	12	51 ± 14	34–84
FNHs	8	0	37 ± 11	22–49	13	1	36 ± 12	14–54
REFs	27	16	45 ± 15	21–78	40	20	41 ± 13	14–70

MV, mean value; *SD*, standard deviation; *HCCs*, hepatocellular carcinomas; *CCCs*, cholangiocellular carcinomas; *CRCs*, metastases of colorectal carcinomas; *BCs*, metastases of breast cancer; *FNHs*, focal nodular hyperplasias; *REFs*, reference (healthy liver tissue)

that was centrally in the lesion and largely unaffected by motion artefacts, pixel misalignments, and susceptibility artefacts. The hand-drawn ROI was carefully placed on the DWI image with $b = 800$ s/mm^2 by adapting the ROI to the most hyperintense structures excluding areas close to the lesion rim to avoid partial-volume effects. Areas with intratumoural necrosis, calcification, haemorrhage, or scar in a FNH were also excluded. After the anatomical position of each ROI was visually cross-checked for pixel misalignments between images with different *b*-values, the ROI was copied into the parameter maps. In case of healthy liver tissue, one large ROI per patient was placed in a central slice into the right lobe, excluding large vessels and benign lesions.

Statistical analysis

Statistical analysis was conducted using SPSS (version 24.0, IBM) and MedCalc (version 18.11, MedCalc Software). As for 1.5-T data [8], analysis of the 3.0-T data was performed on a per-patient basis, whereby mean parameter values were used in case of multiple lesions per patient. Statistical significance ($p < 0.05$) for differences between groups was tested with univariate analysis of variance after proving the Gaussian distribution with the Kolmogorov-Smirnov test. The Levene test showed non-equal variances in the different groups and thus the post hoc Games-Howell test was chosen. ROC analysis was performed for lesion discrimination and dependent ROC curves obtained at 3.0 T were compared with the method of

Table 2 Parameters of the diffusion-weighted imaging (DWI) sequence

Name	Value at 3.0 T	Value at 1.5 T
FOV (RLxAP) / orientation	400 × 352 mm / transversal	380 × 326 mm / transversal
Slice number / thickness / gap	26 / 7.0 mm / 0.7 mm	30 / 7.0 mm / 0.7 mm
Matrix / resolution	132 × 113 / 3.0 × 3.1 mm	112 × 94 / 3.4 × 3.5 mm
Echo time (TE)	44 ms	63 ms
Repetition time (TR)	1 respiratory cycle	1 respiratory cycle
Imaging time per respiration	1894 ms	1600 ms
EPI- / half-Fourier- / SENSE-factor	41 / 0.6 / 3	51 / 0.6 / 2
Diffusion gradients	3 orthogonal directions	3 orthogonal directions
b-values (number of averages per direction)	0,50,250 s/mm^2 (NSA = 2), 800 s/mm^2 (NSA = 4)	0,50,250 s/mm^2 (NSA = 2), 800 s/mm^2 (NSA = 4)
Fat suppression methods	SPIR+SSGR	SPIR
Water-fat shift / BW	11.1 Pixel / 39.0 Hz	9.2 Pixel / 23.6 Hz
BW in EPI frequency direction	3346.0 Hz	1437.9 Hz
Acquisition time	Around 4 min (2:42 min without gating)	Around 4 min (2:42 min without gating)

SENSE, parallel imaging with sensitivity encoding; *FOV*, field of view; *RL*, right-left; *AP*, anterior-posterior; *EPI*, echo-planar imaging; *SPIR*, spectral presaturation by inversion recovery; *SSGR*, slice-selective gradient reversal; *BW*, bandwidth

DeLong et al. Furthermore, the independent ROC curves obtained at 3.0 T and 1.5 T were compared with the method of DeLong et al. For comparison of parameter values obtained at 3.0 T and 1.5 T, an independent samples Student's *t* test (parametric test) was performed for each lesional subgroup separately after proving Gaussian distribution using Kolmogorov-Smirnov test and after variance analysis by the Levene test.

Results

Analysis of IVIM parameters at 3.0 T

Mean parameter values were determined in 143 ROIs placed in 36 HCCs, 5 CCCs, 33 metastases of colorectal carcinomas (CRCs), 20 metastases of breast cancer (BCs), 14 haemangiomas, 8 FNHs, and 27 REFs. Hereby 1/2/3/4/5 lesions per patient were included in 26/2/2/−/− patients with HCCs, 5/−/−/−/− patients with CCCs, 3/4/3/2/1 patients with CRCs, 3/4/3/−/− patients with BCs, 10/2/−/−/− patients with haemangiomas, and 8/−/−/−/− patients with FNHs. In the REF group, 1 ROI per patient was included. Seventy lesions were located in the right and 46 in the left liver lobe. The 27 REFs were located in the right liver lobe. Mean lesion size diameter was 45 mm (10–160 mm). Mean ROI sizes were 540 mm^2 (23–4985 mm^2) in lesions and 1027 mm^2 (413–2911 mm^2) in REFs. Nineteen CRCs and 18 BCs were known to be treated by systemic chemotherapy. Obtained parameter values are given in Table 3, example images in Fig. 2.

According to univariate analysis of variance, differences between groups (6 different liver lesion types, healthy tissue) were statistically significant ($p < 1 \times 10^{-10}$) for all parameters. Results of the post hoc tests are given in Table 4. The main results were as follow: Haemangiomas had the largest values of diffusion sensitive parameters (ADC, D_1', and D_2') in comparison with all other groups, with the exception of non-significant differences in D_2' between haemangiomas and CCCs. FNHs (and REFs) had larger perfusion-sensitive parameters (f_1', f_2', $D^{*\prime}$, ADC_{low}, ADC_{diff}) than all lesion groups, with the exception of non-significant differences in f_2' between FNHs and haemangiomas and in f_2' and $D^{*\prime}$ between FNHs and CCCs.

Results of ROC analysis are given in Table 5. Haemangiomas were best discriminated from all other lesions by D_1' with area under the curve (AUC) of 1.000 and cut-off value of 1501.150×10^{-6} mm^2/s followed by ADC and D_2' with slightly but not significantly lower AUC values. FNHs were best discriminated from all other lesions by f_1' with AUC of 0.993 and cut-off value of 105.650×10^{-3} followed by ADC_{diff}, ADC_{low}, and $D^{*\prime}$ with AUC values not being significantly lower. Discrimination by ADC was also possible but considerably inferior (AUC of 0.764, $p < 0.001$). Benign and malignant lesions were best discriminated by ADC with AUC of 0.968 and cut-off value of 1341.250×10^{-6} mm^2/s followed by D_1' (AUC of 0.909, $p = 0.0107$). All other parameters had significantly lower AUC values. For the ADC cut-off value, 88.8% of the lesions (103 of 116) could be correctly identified as malignant or benign (Fig. 3a). We also

Table 3 Results at 3.0 T of voxel-wise parameter value analysis of conventional apparent diffusion coefficient ADC(0,800), estimations of diffusion coefficient D_1' and D_2', estimations of perfusion fraction f_1' and f_2', pseudodiffusion coefficient $D^{*\prime}$, and perfusion-sensitive parameters ADC_{low} and ADC_{diff} for region of interests (ROI) in healthy liver tissue (REFs), focal nodular hyperplasias (FNHs), haemangiomas (HEMs), hepatocellular carcinomas (HCCs), cholangiocellular carcinomas (CCCs), and metastases of colorectal carcinomas (CRCs) and of breast cancer (BCs). For each group, the mean parameter value (MV), the number of cases (*N*), and the standard deviation (SD) are presented. ADC, *D*, and *D** values are given in units of 10^{-6} mm^2/s and *f* is given in units of 10^{-3}

Groups		ADC	D_1'	D_2'	f_1'	f_2'	$D^{*\prime}$	ADC_{low}	ADC_{diff}
REFs ($N = 27$)	MV	1345	1082	907	184.5	283.5	21488	5221	4407
	SD	139	125	143	35.9	48.7	3819	1109	962
FNHs ($N = 8$)	MV	1381	1190	1011	139.8	250.6	20777	4250	3242
	SD	101	95	140	26.4	59.1	6774	638	620
HEMs ($N = 12$)	MV	1757	1720	1446	46.8	214.9	7450	2387	1162
	SD	211	208	310	37.2	121.1	5720	1173	828
HCCs ($N = 30$)	MV	1130	1065	981	61.9	119.3	10219	2234	1396
	SD	134	120	123	23.4	63.0	3749	615	547
CCCs ($N = 5$)	MV	1109	1058	902	53.1	147.4	11662	2058	1239
	SD	283	266	298	25.5	76.2	3406	672	618
CRCs ($N = 13$)	MV	1052	1048	967	24.4	75.9	5533	1231	547
	SD	181	190	198	11.1	20.5	2475	378	244
BCs ($N = 10$)	MV	1157	1107	969	45.7	138.6	7156	1906	1058
	SD	145	155	136	23.6	34.2	2752	516	468

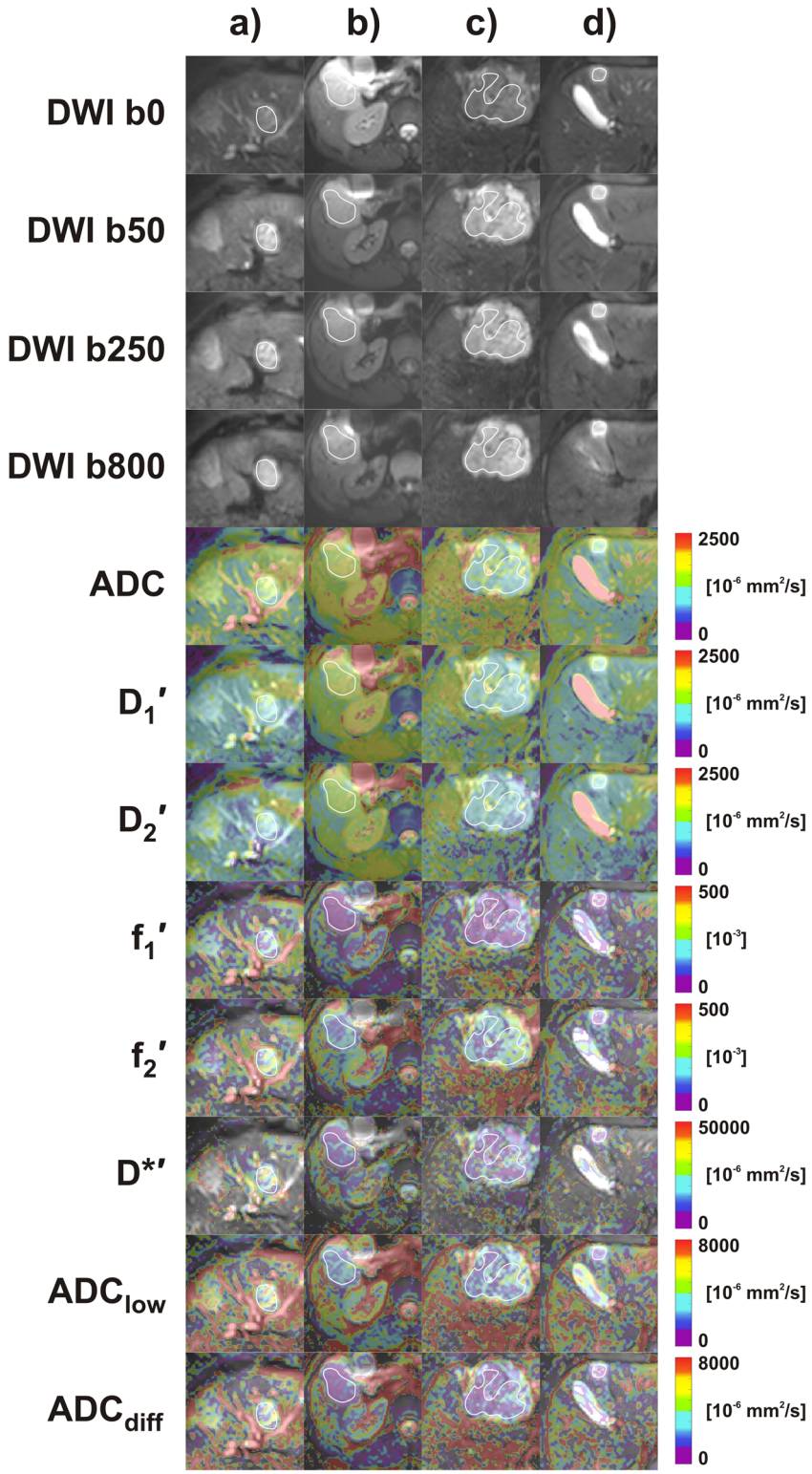

Fig. 2 Typical examples of intravoxel incoherent motion (IVIM)–based parameter maps for different liver lesions at 3.0 T. From left to right, images for focal nodular hyperplasia (FNH) and two haemangiomas (**a**), multifocal hepatocellular carcinoma (HCC) (**b**), and metastases of colorectal carcinoma (CRCs) (**c**) and breast cancer (BCs) (**d**) are shown. Original diffusion-weighted images with $b = 0$, 50, 250, 800 s/mm^2 are presented together with conventional ADC, diffusion-sensitive D_1' and D_2' parameter maps, and perfusion-sensitive f_1', f_2', $D^{*\prime}$, ADC_{low}, ADC_{diff} parameter maps. The parameter maps are displayed as colour-coded overlays over DWI $b = 0$. If bad data quality due to voxel misalignment, motion influence, or limited SNR led to negative parameter values especially for f_1' or f_2' or to not defined values of the ln(x) in the equation for $D^{*\prime}$, these voxels were not colorised. Regions of interest analysed are marked in white (haemangiomas, HCC, CRC, BC) and yellow (FNH). The FNH reveals medium diffusion and high perfusion parameter values, similar to healthy liver tissue not including large vessels. The haemangiomas show high values of diffusion parameters in combination with very low values of perfusion parameters. Malignant lesions (HCC, CRC, and BC) exhibit similar or slightly lower diffusion parameter than healthy tissue or FNH in combination with low perfusion parameters

used a combination of D_1' and f_1' parameters for the discrimination between benign and malignant lesions. Hereby the cut-off values obtained for discrimination of haemangiomas and FNHs were used (1501.150×10^{-6} mm^2/s and 105.650×10^{-3}, respectively). Lesions with D_1' and f_1' values lower than the cut-off values were assigned as malignant and lesions with D_1' or f_1' values higher than the cut-off values, as benign. For this parameter combination, 99.1% of the lesions (115 of 116) were correctly identified as malignant and benign (Fig. 3b, c).

Table 4 Results at 3.0 T of post hoc Games-Howell tests for detecting differences among the following groups: Healthy liver tissue (REFs), focal nodular hyperplasias (FNHs), haemangiomas (HEMs), hepatocellular carcinomas (HCCs), cholangiocellular carcinomas (CCCs), and metastases of colorectal carcinomas (CRCs) and breast cancer (BCs). Given are the *p* values of the conventional apparent diffusion coefficient ADC, estimations of diffusion coefficient D_1' and D_2', estimations of perfusion fraction f_1' and f_2', pseudodiffusion coefficient D*′ and perfusion sensitive parameters ADC_{low} and ADC_{diff}

Compared groups	ADC	D_1'	D_2'	f_1'	f_2'	$D^{*\prime}$	ADC_{low}	ADC_{diff}
REF-FNH	Ns	Ns	Ns	2.0E-02	Ns	Ns	Ns	1.1E-02
REF-HEM	2.5E-04	1.3E-06	9.4E-04	1.3E-08	Ns	1.7E-05	1.3E-05	1.9E-09
REF-HCC	4.0E-06	Ns	Ns	7.1E-13	6.4E-13	6.2E-13	8.3E-13	7.7E-13
REF-CCC	Ns	Ns	Ns	2.1E-04	Ns	1.0E-02	2.0E-04	1.4E-04
REF-CRC	8.9E-04	Ns	Ns	6.7E-13	6.5E-13	6.7E-13	6.9E-13	7.5E-13
REF-BC	3.6E-02	Ns	Ns	1.1E-11	1.1E-08	2.4E-10	2.1E-12	7.9E-13
FNH-HEM	9.1E-04	1.3E-05	8.5E-03	6.8E-05	Ns	6.7E-03	3.8E-03	9.2E-05
FNH-HCC	6.6E-04	Ns	Ns	2.4E-04	2.1E-03	2.8E-02	1.1E-04	2.2E-02
FNH-CCC	Ns	Ns	Ns	3.0E-03	Ns	Ns	4.0E-03	4.2E-03
FNH-CRC	6.4E-04	Ns	Ns	1.9E-05	4.8E-04	3.0E-03	3.6E-06	2.3E-05
FNH-BC	2.0E-02	Ns	Ns	2.4E-05	8.1E-03	5.8E-03	1.7E-05	2.8E-05
HEM-HCC	1.8E-06	1.2E-06	3.6E-03	Ns	Ns	Ns	Ns	Ns
HEM-CCC	3.2E-02	2.1E-02	Ns	Ns	Ns	Ns	Ns	Ns
HEM-CRC	1.8E-07	4.4E-07	3.5E-03	Ns	Ns	Ns	Ns	Ns
HEM-BC	3.3E-06	2.8E-06	3.1E-03	Ns	Ns	Ns	Ns	Ns
HCC-CCC	Ns	Ns	Ns	Ns	Ns	Ns	Ns	Ns
HCC-CRC	Ns	Ns	Ns	2.5E-07	2.6E-02	5.2E-04	2.8E-06	3.0E-07
HCC-BC	Ns	Ns	Ns	Ns	Ns	Ns	Ns	Ns
CCC-CRC	Ns	Ns	Ns	Ns	Ns	Ns	Ns	Ns
CCC-BC	Ns	Ns	Ns	Ns	Ns	Ns	Ns	Ns
CRC-BC	Ns	Ns	Ns	Ns	2.3E-03	Ns	4.0E-02	Ns

When excluding CRCs and BCs to avoid the potential influence of treatment, similar results were obtained compared with the whole data set: For an ADC cut-off point of 1341.250×10^{-6} mm^2/s, 92.1% of the lesions (58 of 63) were correctly identified as malignant and benign. For a combination of D_1' cut-off value of 1431.100×10^{-6} mm^2/s and f_1' cut-off value of 105.650×10^{-3}, 100.0% of the lesions (63 of 63) were correctly identified as malignant and benign.

Comparison between 3.0 T and 1.5 T

The comparison of ROC curves obtained at 3.0 T and 1.5 T revealed a slightly, but not significantly, higher AUC for the discrimination between haemangiomas and all other lesions by D_1' (AUC of 1.000 vs 0.994, $p = 0.163$) and between FNHs and all other lesions by f_1' (AUC of 0.993 vs 0.989, $p = 0.737$). For the discrimination between malignant and benign lesions, at 3.0 T, a significantly higher AUC was found for f_2' (AUC of 0.831 vs 0.630, $p = 0.024$) and a trend of higher AUC for ADC (AUC of 0.968 vs 0.915, $p = 0.102$) and D_1' (AUC of 0.909 vs 0.858, $p = 0.364$). All other parameters showed non-significant AUC differences. The comparison of the parameter values between 3.0 T and 1.5 T revealed no significant differences for most lesion groups (REFs, FNHs, haemangiomas, CCCs, BCs). For HCCs, a tendency of larger *D*(250,800) and lower *f*(250,800) was found at 3.0 T ($p = 0.019$ and $p = 0.048$, respectively). For CRCs, all perfusion-sensitive parameters were lower at 3.0 T (p value of 0.009 for ADC(0,800), < 0.00001 for *f*(50,800), 0.001 for *f*(250,800), 0.001 for *D**, < 0.000001 for ADC(0,50), and 0.00001 for ADC_{diff}). Moreover, the standard deviations within the ROIs (RSDs) did not differ between 3.0 T and 1.5 T for most lesion groups (FNHs, haemangiomas, HCCs, CCCs, BCs), see Table 6. Lower RSD values at 3.0 T compared with 1.5 T were only found for REFs in case of ADC(0,800) ($p = 0.035$), *D*(250,800) ($p = 0.019$), *f*(50,800) ($p = 0.021$), *f*(250,800) ($p = 0.008$), ADC(0,50) ($p = 0.024$), and ADC_{diff} ($p = 0.038$) and for CRC in case of ADC(0,800) ($p < 0.001$), *D*(50,800) ($p < 0.001$), *D*(250,800) ($p < 0.0001$), *f*(50,800) ($p = 0.001$), *D** ($p = 0.046$), ADC(0,50) ($p = 0.002$), and ADC_{diff} ($p < 0.001$). The inter-individual standard deviations of the parameters for the different lesion groups at 3.0 T were similar or lower than at 1.5 T.

Discussion

The main result of the present basic study is that simplified IVIM for liver lesion characterisation at 3.0 T achieved excellent accuracy in differentiating malignant from benign lesions by using the combination of parameters *D* and *f* approximated from $b = 0$, 50, 800 s/mm^2 (D_1', f_1'). Compared with 1.5 T, the achieved accuracy tended to be higher at 3.0 T [8]. All other parameters, including the conventional ADC calculated from $b = 0$ and 800 s/mm^2, the approximations of *D* and *f* from *b* =

Table 5 Results of the receiver operating characteristic analysis of all 3.0-T data (a) and of the reduced 3.0-T data set (without CRCs and BCs to avoid treatment influences of former systemic chemotherapy) (b). The optimal cut-off point according to the Youden index is given in 10^{-6} mm^2/s for ADC, D_1', D_2', $D^{*\prime}$, ADC_{low}, and ADC_{diff} and in 10^{-3} for f_1' and f_2', whereby a higher test result indicates a more "positive" test (a negative test direction is marked with a number sign)

Test variable	AUC	Std. Err.	A. Sign.	Asym. 95% C. I.		Cut-off point	Sen.	1-Spec.	Accur.
				LB	UB				
a) All data									
Haemangiomas ($n = 12$) vs all other lesions ($n = 66$)									
ADC	0.999	0.002	4.5E-08	0.995	1.000	1490.400	1.000	0.015	0.992
D_1'	1.000	0.000	4.2E-08	1.000	1.000	1501.150	1.000	0.000	1.000
D_2'	0.907	0.061	8.2E-06	0.788	1.000	1238.300	0.833	0.015	0.909
$f_1'^{\#}$	0.593	0.093	3.1E-01	0.224	0.589				
f_2'	0.714	0.097	1.9E-02	0.523	0.905	254.400	0.500	0.045	0.727
$D^{*\prime\#}$	0.635	0.101	1.4E-01	0.167	0.563				
ADC_{low}	0.588	0.096	3.3E-01	0.400	0.777				
$ADC_{diff}^{\#}$	0.566	0.092	4.7E-01	0.254	0.614				
FNHs ($n = 8$) vs all other lesions ($n = 70$)									
ADC	0.764	0.052	1.5E-02	0.663	0.866	1233.250	1.000	0.357	0.821
D_1'	0.639	0.069	2.0E-01	0.505	0.774				
$D_2'^{\#}$	0.507	0.099	9.5E-01	0.299	0.687				
f_1'	0.993	0.008	5.5E-06	0.977	1.000	105.650	1.000	0.014	0.993
f_2'	0.882	0.038	4.2E-04	0.807	0.958				
$D^{*\prime}$	0.950	0.032	3.3E-05	0.888	1.000				
ADC_{low}	0.991	0.010	5.9E-06	0.972	1.000	3480.400	1.000	0.014	0.993
ADC_{diff}	0.993	0.008	5.5E-06	0.977	1.000	2477.700	1.000	0.014	0.993
Benign ($n = 20$) vs malignant ($n = 58$) lesions									
ADC	0.968	0.017	5.2E-10	0.934	1.000	1341.250	0.900	0.069	0.916
D_1'	0.909	0.038	5.8E-08	0.834	0.983	1177.850	0.850	0.172	0.839
D_2'	0.774	0.069	2.7E-04	0.639	0.910	1138.000	0.650	0.121	0.765
f_1'	0.674	0.085	2.1E-02	0.507	0.841	105.650	0.450	0.000	0.725
f_2'	0.831	0.064	1.1E-05	0.706	0.955	141.400	0.850	0.207	0.822
$D^{*\prime}$	0.625	0.091	9.7E-02	0.447	0.803				
ADC_{low}	0.797	0.072	7.9E-05	0.656	0.939	3058.700	0.600	0.017	0.791
ADC_{diff}	0.693	0.082	1.0E-02	0.532	0.854	2477.700	0.450	0.000	0.725
b) Reduced data set (without CRCs and BCs)									
Haemangiomas ($n = 12$) vs all other lesions ($n = 43$)									
ADC	0.998	0.003	1.6E-07	0.992	1.000	1484.800	1.000	0.023	0.988
D_1'	1.000	0.000	1.5E-07	1.000	1.000	1431.100	1.000	0.000	1.000
D_2'	0.909	0.064	1.7E-05	0.784	1.000	1231.350	0.833	0.000	0.917
$f_1'^{\#}$	0.703	0.090	3.2E-02	0.527	0.880	38.100	0.500	0.116	0.692
f_2'	0.679	0.102	5.9E-02	0.480	0.878				
$D^{*\prime\#}$	0.719	0.095	2.1E-02	0.533	0.905	5506.950	0.500	0.047	0.727
$ADC_{low}^{\#}$	0.510	0.099	9.2E-01	0.295	0.685				
$ADC_{diff}^{\#}$	0.676	0.089	6.4E-02	0.149	0.499				
FNHs ($n = 8$) vs all other lesions ($n = 47$)									
ADC	0.694	0.067	8.1E-02	0.563	0.825				
D_1'	0.580	0.077	4.7E-01	0.428	0.731				
$D_2'^{\#}$	0.572	0.097	5.2E-01	0.238	0.619				
f_1'	0.989	0.012	1.1E-05	0.966	1.000	105.650	1.000	0.021	0.989
f_2'	0.830	0.054	3.1E-03	0.723	0.936	169.700	1.000	0.255	0.872
$D^{*\prime}$	0.928	0.044	1.2E-04	0.841	1.000	14,232.750	0.875	0.128	0.874

Table 5 (continued)

Test variable	AUC	Std. Err.	A. Sign.	Asym. 95% C. I.		Cut-off point	Sen.	1-Spec.	Accur.
				LB	UB				
ADC_{low}	0.987	0.014	1.2E-05	0.959	1.000	3480.400	1.000	0.021	0.989
ADC_{diff}	0.989	0.012	1.1E-05	0.966	1.000	2477.700	1.000	0.021	0.989
Benign ($n = 20$) vs malignant ($n = 35$) lesions									
ADC	0.971	0.019	7.8E-09	0.934	1.000	1341.250	0.900	0.057	0.921
D_1'	0.911	0.040	4.7E-07	0.832	0.990	1177.850	0.850	0.171	0.839
D_2'	0.763	0.074	1.3E-03	0.618	0.908	1127.250	0.650	0.143	0.754
f_1'	0.613	0.094	1.7E-01	0.429	0.797				
f_2'	0.809	0.067	1.5E-04	0.677	0.941	140.400	0.850	0.257	0.796
$D^{*\prime}$	0.569	0.095	4.0E-01	0.382	0.755				
ADC_{low}	0.754	0.080	1.8E-03	0.597	0.912	3058.700	0.600	0.029	0.786
ADC_{diff}	0.633	0.091	1.0E-01	0.455	0.811				

AUC, area under the curve; *Std. Err.*, standard error (under the non-parametric assumption); *A. Sign.*, asymptotic significance (null hypothesis: true area = 0.5); *Asym. 95% C. I.*, asymptotic 95% confidence interval; *LB*, lower bound; *UP*, upper bound; *Sen.*, sensitivity; *Spec.*, specificity; *Accur.*, accuracy (= (Sen. + Spec.)/2)

0, 250, 800 s/mm^2 (D_2', f_2'), and $D^{*\prime}$ derived from four *b*-values turned out to be clearly inferior to the combined D_1' and f_1'.

Up to now, there are only a few studies using a stable IVIM parameter analysis method like segmented fitting or explicitly calculating formulas in order to differentiate between subgroups of malignant and benign lesions, and this is the first study on simplified IVIM at 3.0 T [8, 9, 13–17, 19]. For lesion differentiation, the same parameters turned out to be optimal and the same combination of *b*-values was found as for simplified IVIM at 1.5 T. Furthermore, the cut-off values at 3.0 T for the discrimination between malignant and benign lesions were very similar to those at 1.5 T [8]. Diffusion-sensitive parameters were highest for haemangiomas with D_1' and ADC being the best single parameters to differentiate them from all other lesions. Perfusion-sensitive parameters were higher for FNHs than for HCCs, CCCs, metastases, and haemangiomas with f_1' being most suitable to differentiate FNHs from all other lesions. The lower $D^{*\prime}$ and lower f_1' and f_2' values in malignant lesions may be caused by slow or stagnant blood flow through damaged tumour vessels and low density and/or diameter of microvascular vessels containing flowing blood as discussed in detail earlier [8]. For haemangiomas, this finding can possibly be explained by the presence of dilated vessels and pools of stagnant blood leading to low $D^{*\prime}$ values [8]. If $D^{*\prime}$ is in the order of D_2', the

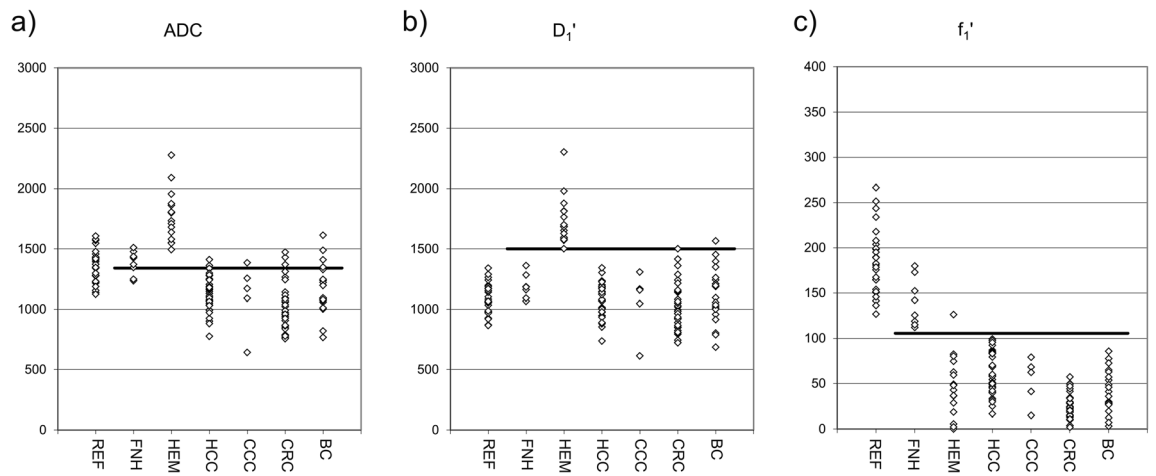

Fig. 3 Overview to ADC (**a**), D_1' (**b**), and f_1' (**c**) values measured in healthy liver tissue (REFs), focal nodular hyperplasias (FNHs), haemangiomas (HEMs), hepatocellular carcinomas (HCCs), cholangiocellular carcinomas (CCCs), and metastases of colorectal carcinomas (CRCs) and breast cancer (BCs) at 3.0 T. For an ADC cut-off value of 1341.250×10^{-6} mm^2/s (black line in (a)), 88.8% of the lesions (103 of 116) were correctly identified as malignant and benign. For a combination of D_1' cut-off value of 1501.150×10^{-6} mm^2/s (black line in (b)) and f_1' cut-off value of 105.650×10^{-3} (black line in (c)), 99.1% of the lesions (115 of 116) were correctly identified

Table 6 Standard deviations of the parameter values within the analysed region of interests (RSDs) at 3.0 T and 1.5 T. The mean values (MV) of RSDs and the number of analysed ROIs (*N*) are presented for conventional apparent diffusion coefficient ADC(0,800), estimations of diffusion coefficient D_1' and D_2', estimations of perfusion fraction f_1' and f_2', pseudodiffusion coefficient $D^{*\prime}$, and perfusion-sensitive parameters ADC_{low} and ADC_{diff} in focal nodular hyperplasias (FNHs), haemangiomas (HEMs), hepatocellular carcinomas (HCCs), cholangiocellular carcinomas (CCCs), and metastases of colorectal carcinomas (CRCs) and of breast cancer (BCs). RSDs of ADC, *D*, and *D** values are given in units of 10^{-6} mm^2/s and RSDs of *f* are given in units of 10^{-3}. Significantly different values are marked in italics

Groups		RSD ADC	RSD D_1'	RSD D_2'	RSD f_1'	RSD f_2'	RSD $D^{*\prime}$	RSD ADC_{low}	RSDADC_{diff}
REFs	MV 3.0 T (*N* = 27)	*178*	132	*183*	*85.3*	*102.3*	15354	*2231*	*2224*
	MV 1.5 T (*N* = 40)	*215*	159	*230*	*101.2*	*123.9*	17518	*2748*	*2707*
FNHs	MV 3.0 T (*N* = 8)	123	100	131	53.9	65.8	12156	1281	1287
	MV 1.5 T (*N* = 19)	124	103	127	57.6	66.1	15359	1358	1377
HEMs	MV 3.0 T (*N* = 14)	150	126	146	31.9	75.6	7304	890	779
	MV 1.5 T (*N* = 24)	184	153	173	39.1	77.8	7434	1145	907
HCCs	MV 3.0 T (*N* = 36)	148	135	158	50.6	74.9	13016	1255	1138
	MV 1.5 T (*N* = 44)	145	131	145	44.9	65.2	11748	1102	1013
CCCs	MV 3.0 T (*N* = 5)	147	126	133	46.2	63.9	12664	1158	1061
	MV 1.5 T (*N* = 11)	210	192	212	41.5	53.6	11696	1159	921
CRCs	MV 3.0 T (*N* = 33)	*159*	*146*	*143*	*30.7*	58.8	*9168*	*890*	*677*
	MV 1.5 T (*N* = 45)	*224*	*207*	*206*	*44.8*	66.0	*11148*	*1174*	*1001*
BCs	MV 3.0 T (*N* = 20)	176	165	166	38.7	67.6	7999	1006	875
	MV 1.5 T (*N* = 30)	187	177	186	40.2	63.1	9621	1026	899

perfusion influence is not negligible at high *b*-values and the behaviour of ln(*S*(*b*)) is also non-linear for high *b*-values [15]. Compared with healthy liver tissue, FNHs had similar $D^{*\prime}$ values, but slightly lower values of f_1', f_2', ADC_{low}, and ADC_{diff}, because perfusion fraction is lower as a result from the longer relaxation times T1 and T2 as previously reported [8]. FNHs may reveal similar microcirculation properties as normal liver tissue because of its hyperplastic rather than neoplastic nature [8]. In order to discriminate malignant from benign lesions, the highest accuracy was obtained by ADC followed by D_1' with significantly higher values in benign lesions. By combining D_1' and f_1', discriminatory power for differentiation between benign and malignant lesions further improved.

Comparing field strengths with respect to diagnostic accuracy for discriminating between malignant and benign lesions, 3.0 T tended to be superior in comparison with 1.5 T. By using the combination of D_1' and f_1', 99.1% of the lesions could be correctly identified as malignant or benign at 3.0 T compared with 85.6% at 1.5 T [8]. For the single parameters ADC and D_1', AUC values of 0.968 vs 0.915 ($p = 0.102$) and 0.909 vs 0.858 ($p = 0.364$), respectively, were found at 3.0 T compared with 1.5 T [8]. Based on only the ADC, 88.8% of the lesions could be correctly identified as malignant and benign at 3.0 T in comparison with 82.1% at 1.5 T [8]. In concordance to this finding, in previous studies, discriminatory power between benign and malignant lesions was found to be high at 3.0 T (AUC of *D*, 0.98 at 3.0 T [9]) and low at 1.5 T (AUC of *D*, 0.723 [14]). In both studies, benign lesion group composition was comparable to our study (containing haemangiomas and focal nodular hyperplasias). However, if the benign lesion group contained also cysts or only haemangiomas (high ADC and *D* values), high AUC values were not only obtained at 3.0 T (0.933–0.98 for ADC and 0.96–0.971 for *D* [12]) but also at 1.5 T (0.967 for ADC and 0.837–0.98 for *D* [10, 16]). For the discrimination between malignant and benign lesions using perfusion parameters, for f_2', a significantly higher AUC was found in the present 3.0-T study as compared with 1.5 T (0.831 compared with 0.630, $p = 0.024$) [8]. The discriminatory power of perfusion parameters was significantly lower than for diffusion parameters, at both field strengths 3.0 and 1.5 T. This can be explained due to the fact that some benign lesions as cysts and haemangiomas have low values of perfusion parameters, which are within the range of the malignant lesions. The tendency toward higher diagnostic accuracy at 3.0 T for the differentiation between malignant and benign lesions might be caused by (a) changes of measured perfusion parameters due to different relaxation times and TE values, (b) slight differences in group compositions, or (c) improved signal-to-noise ratio (SNR) and/or image quality. For clarification of (a), parameter values obtained in this study were directly compared with those obtained in the previous 1.5-T study [8]. However, no significant differences could be found for REFs, FNHs, haemangiomas, CCCs, and BCs, neither for the diffusion nor for the perfusion parameters. In general, the perfusion fraction and parameters influenced by the perfusion fraction might have different values at 1.5 T and 3.0 T, depending on the relaxation times and chosen TE values [27]. Different values of the perfusion fraction might have caused differences in diagnostic

accuracy. By using a smaller TE at 3.0 T, changes in relaxation times have apparently been compensated. Only for CRCs, lower perfusion parameters and lower RSDs were found at 3.0 T. This may be explained by a larger amount of partially necrotic CRCs due to systemic treatment in this study (58% at 3.0 T, 9% at 1.5 T). Necrotic changes might lead to lower D^* values and reduced heterogeneity within the lesions [5, 28]. For BCs, a similar number of treated lesions were included at 3.0 T and 1.5 T (90% at 3.0 T and 87% at 1.5 T) not leading to any differences. Explanation (b) is also rather unlikely if one considers that two different compositions of the malignant lesion group (with and without metastases) lead to similar results. As an additional test, we re-investigated discriminability at 1.5 T for a smaller benign lesion group with the same number of FNHs and haemangiomas as at 3.0 T (data not shown); however, AUC values did not increase but decline. Thus, explanation (c), the improved SNR and/or image quality, might be most relevant. Diffusion parameters at 1.5 T are not significantly larger than those at 3.0 T which does not speak for SNR limitations at 1.5 T. However, RSD values for healthy tissue are larger at 1.5 T compared with 3.0 T which might indicate lower SNR at 1.5 T. Furthermore, the inter-individual standard deviations of the parameters for the different groups were larger at 1.5 T what could be caused by lower measurement repeatability/reproducibility. In general, the image quality of DWI at 3.0 T is rather lower due to more prominent dielectric shading (e.g. in patients with ascites), more pronounced susceptibility and motion artefacts, and less uniform fat suppression [29–32]. However, in the present study, two advanced technologies were used to improve DWI image quality at 3.0 T, dual-source parallel RF excitation and transmission technology for improving RF uniformity and a combination of SPIR with slice-selective gradient reversal (SSGR) for improved fat suppression [29, 30, 33].

The results of the present study and the 1.5-T study [8] confirm the usefulness of the three *b*-value approaches chosen in previous 1.5-T studies on lesion characterisation [15, 17] and assessment of therapy [22–25]. D_1' and f_1' serve as standardised empirical biomarkers indicating non-specific tissue alteration or therapy response. The numerically stable, voxel-wise determination enables a visual assessment of heterogeneous lesions and the targeted quantitative analysis of necrotic or viable areas. The high diagnostic accuracy of 99.1% of correctly identified malignant and benign lesions at 3.0 T and 85.5% at 1.5 T is very promising and motivates future studies, e.g. a field strength comparison for measured parameter reproducibility. Moreover, it would be interesting to further evaluate the clinical impact of simplified IVIM for lesion characterisation with respect to the following questions: Is simplified IVIM suitable to replace contrast-enhanced images in certain cases as a "fast-MRI" perspective? And is the method based on the determined threshold values suitable to also correctly classify rarer and more atypical lesions?

General concerns regarding the simplified IVIM approach as for example the *b*-value choice have already been addressed in the previous 1.5-T study [8]. A limitation of the study is that only patients with common lesion types and definitive diagnosis (typical MRI findings or histologically proven) have been included. However, this design was chosen in order to basically evaluate the simplified IVIM approach. Another limitation is the inter-individual comparison of diagnostic accuracy between 3.0 T and 1.5 T.

The authors use now and would recommend to use *b*-values of 0, 50, and 800 s/mm^2 for liver DWI.

In conclusion, simplified IVIM is suitable for lesion characterisation at 3.0 T with a tendency toward superior diagnostic accuracy for discriminating between malignant and benign lesions compared with 1.5 T. The combination of IVIM parameters D and f approximated from *b*-values 0, 50, and 800 s/mm^2 provided more discriminatory power than the ADC determined from two *b*-values, D and f approximated from 0, 250, and 800 s/mm^2, and D^* approximated from four *b*-values.

Funding The authors state that this work has not received any funding.

Compliance with ethical standards

Guarantor The scientific guarantor of this publication is Petra Mürtz.

Conflict of interest The authors of this manuscript declare no relationships with any companies, whose products or services may be related to the subject matter of the article.

Statistics and biometry No complex statistical methods were necessary for this paper.

Informed consent Written informed consent was waived by the Institutional Review Board.

Ethical approval Institutional Review Board approval was obtained.

Study subjects or cohorts overlap Some study subjects or cohorts have been previously reported in Mürtz P, Sprinkart AM, Reick M, et al (2018) Accurate IVIM model-based liver lesion characterisation can be achieved with only three b-value DWI. Eur Radiol. doi: https://doi.org/10.1007/s00330-018-5401-7.

Methodology
- retrospective
- diagnostic study
- performed at one institution

References

1. Le Bihan D, Breton E, Lallemand D, Aubin ML, Vignaud J, Laval-Jeantet M (1988) Separation of diffusion and perfusion in intravoxel incoherent motion MR imaging. Radiology 168:497–505

2. Koh DM, Collins DJ, Orton MR (2011) Intravoxel incoherent motion in body diffusion-weighted MRI: reality and challenges. AJR Am J Roentgenol 196:1351–1361
3. Padhani AR, Liu G, Koh DM et al (2009) Diffusion-weighted magnetic resonance imaging as a cancer biomarker: consensus and recommendations. Neoplasia 11:102–125
4. Takahara T, Kwee TC (2012) Low b-value diffusion-weighted imaging: emerging applications in the body. J Magn Reson Imaging 35:1266–1273
5. Taouli B, Koh DM (2010) Diffusion-weighted MR imaging of the liver. Radiology 254:47–66
6. Aoyagi T, Shuto K, Okazumi S et al (2012) Apparent diffusion coefficient correlation with oesophageal tumour stroma and angiogenesis. Eur Radiol 22:1172–1177
7. Cho GY, Kim S, Jensen JH et al (2012) A versatile flow phantom for intravoxel incoherent motion MRI. Magn Reson Med 67:1710–1720
8. Mürtz P, Sprinkart AM, Reick M et al (2018) Accurate IVIM model-based liver lesion characterisation can be achieved with only three b-value DWI. Eur Radiol 28:4418–4428
9. Wang M, Li X, Zou J et al (2016) Evaluation of hepatic tumors using intravoxel incoherent motion diffusion-weighted MRI. Med Sci Monit 22:702–709
10. Zhu L, Cheng Q, Luo W et al (2015) A comparative study of apparent diffusion coefficient and intravoxel incoherent motion-derived parameters for the characterization of common solid hepatic tumors. Acta Radiol 56:1411–1418
11. Yoon JH, Lee JM, Yu MH et al (2014) Evaluation of hepatic focal lesions using diffusion-weighted MR imaging: comparison of apparent diffusion coefficient and intravoxel incoherent motion-derived parameters. J Magn Reson Imaging 39:276–285
12. Watanabe H, Kanematsu M, Goshima S et al (2014) Characterizing focal hepatic lesions by free-breathing intravoxel incoherent motion MRI at 3.0 T. Acta Radiol 55:1166–1173
13. Colagrande S, Regini F, Pasquinelli F et al (2013) Focal liver lesion classification and characterization in noncirrhotic liver: a prospective comparison of diffusion-weighted magnetic resonance–related parameters. J Comput Assist Tomogr 37:560–567
14. Doblas S, Wagner M, Leitao HS et al (2013) Determination of malignancy and characterization of hepatic tumor type with diffusion-weighted magnetic resonance imaging: comparison of apparent diffusion coefficient and intravoxel incoherent motion–derived measurements. Invest Radiol 48:722–728
15. Penner A-H, Sprinkart AM, Kukuk GM et al (2013) Intravoxel incoherent motion model-based liver lesion characterisation from three b-value diffusion-weighted MRI. Eur Radiol 23:2773–2783
16. Ichikawa S, Motosugi U, Ichikawa T et al (2013) Intravoxel incoherent motion imaging of focal hepatic lesions. J Magn Reson Imaging 37:1371–1376
17. Coenegrachts K, Delanote J, Ter Beek L et al (2009) Evaluation of true diffusion, perfusion factor, and apparent diffusion coefficient in non-necrotic liver metastases and uncomplicated liver hemangiomas using black-blood echo planar imaging. Eur J Radiol 69:131–138
18. Yamada I, Aung W, Himeno Y et al (1999) Diffusion coefficients in abdominal organs and hepatic lesions: evaluation with intravoxel incoherent motion echo-planar MR imaging. Radiology 210:617–623
19. Luo M, Zhang L, Jiang X, Zhang W (2017) Intravoxel incoherent motion diffusion-weighted imaging: evaluation of the differentiation of solid hepatic lesions. Transl Oncol 10:831–838
20. Andreou A, Koh DM, Collins DJ et al (2013) Measurement reproducibility of perfusion fraction and pseudodiffusion coefficient derived by intravoxel incoherent motion diffusion-weighted MR imaging in normal liver and metastases. Eur Radiol 23:428–434
21. Kakite S, Dyvorne H, Besa C et al (2015) Hepatocellular carcinoma: short-term reproducibility of apparent diffusion coefficient and intravoxel incoherent motion parameters at 3.0T. J Magn Reson Imaging 41:149–156
22. Mürtz P, Penner A-H, Pfeiffer A-K et al (2016) Intravoxel incoherent motion model-based analysis of diffusion-weighted magnetic resonance imaging with 3 b-values for response assessment in locoregional therapy of hepatocellular carcinoma. Onco Targets Ther 9:6425–6433
23. Pieper CC, Sprinkart AM, Meyer C et al (2016) Evaluation of a simplified intravoxel incoherent motion (IVIM) analysis of diffusion-weighted imaging for prediction of tumor size changes and imaging response in breast cancer liver metastases undergoing radioembolization: a retrospective single center analysis. Medicine (Baltimore) 95:1–9
24. Pieper CC, Willinek WA, Meyer C et al (2016) Intravoxel incoherent motion diffusion-weighted MR imaging for prediction of early arterial blood flow stasis in radioembolization of breast cancer liver metastases. J Vasc Interv Radiol 27:1320–1328
25. Pieper C, Meyer C, Sprinkart AM et al (2016) The value of intravoxel incoherent motion model-based diffusion-weighted imaging for outcome prediction in resin-based radioembolization of breast cancer liver metastases. Onco Targets Ther 9:4089–4098
26. Bruix J, Sherman M, American Association for the Study of Liver Disease (2011) Management of hepatocellular carcinoma: an update. Hepatology 53:1020–1022
27. Lemke A, Laun FB, Simon D et al (2010) An in vivo verification of the intravoxel incoherent motion effect in diffusion-weighted imaging of the abdomen. Magn Reson Med 64:1580–1585
28. Wagner M, Doblas S, Daire JL et al (2012) Diffusion-weighted MR imaging for the regional characterization of liver tumors. Radiology 264:464–472
29. Mürtz P, Kaschner M, Träber F et al (2012) Diffusion-weighted whole-body MRI with background body signal suppression: technical improvements at 3.0 T. J Magn Reson Imaging 35:456–461
30. Mürtz P, Kaschner M, Träber F et al (2012) Evaluation of dual-source parallel RF excitation for diffusion-weighted whole-body MR imaging with background body signal suppression at 3.0 T. Eur J Radiol 81:3614–3623
31. Willinek WA, Gieseke J, Kukuk GM et al (2010) Dual-source parallel radiofrequency excitation body MR imaging compared with standard MR imaging at 3.0 T: initial clinical experience 1. Radiology 256:966–975
32. Chang JM, Lee JM, Lee MW et al (2006) Superparamagnetic iron oxide-enhanced liver magnetic resonance imaging: comparison of 1.5 T and 3.0 T imaging for detection of focal malignant liver lesions. Invest Radiol 41:168–174
33. Horie T, Ogino T, Muro I et al (2009) Optimization of fat suppression for 3.0T DWIBS. In: 17th Annual ISMRM Scientific Meeting and Exhibition 2009. pp 4614. Honolulu, Hawaii